The International Archives of the Photogrammetry, Remote Sensing and Spatial Information Sciences, Volume XLVIII-M-9-2025
30th CIPA Symposium “Heritage Conservation from Bits:
From Digital Documentation to Data-driven Heritage Conservation”, 25–29 August 2025, Seoul, Republic of Korea

FEM Simulation of Ballistic Impacts on Pompeii Walls for the Reconstruction of Roman Throwers War Machine

Monil Mihirbhai Thakkar[1], Amir Ardeshiri Lordejani[1], Mario Guagliano[1], Silvia Bertacchi[2], Sara Gonizzi Barsanti[2], Adriana Rossi[2]

[1] Dept. of Mechanical Engineering, Politecnico di Milano, via la Masa 1, 20156, Milan, Italy
- (monilmihirbhai.thakkar, amir.ardeshiri, mario.guagliano)@polimi.it
[2] Dept. of Engineering, Università degli Studi della Campania Luigi Vanvitelli, via Roma 29, 81031, Aversa (CE), Italy
- (silvia.bertacchi, sara.gonizzibarsanti, adriana.rossi)@unicampania.it

Abstract

Beginning with the visible dents observed on the fortified walls of Pompeii, a reverse engineering methodology is employed to uncover the engineering principles behind the design of Roman military devices, which played a crucial role in their conquests across the empire. In this context, utilizing photogrammetric data collected through experimental recordings, the study aims to simulate projectile impacts on Grey Tuff to estimate the velocities at impact and the resulting penetration depths. This provides valuable insights into the destructive capabilities of Roman weaponry. Material behaviour models are developed and integrated into finite element analyses. The process includes mesh convergence testing, calibration of impact velocities, and examination of impact angles to determine the launch conditions of projectiles that align with the observed damage patterns. Based on these findings, the study offers guidelines for the design principles underlying Roman war machines, contributing to a better understanding of their construction and effectiveness.

Keywords: Pompei Historical Site, Finite Element Analysis, Material Modelling, Wall impact analysis, Concrete Damage Plasticity (CDP)

1. Introduction

In recent decades, the spread of digital acquisition techniques in the field of cultural heritage, has offered numerous advantages, making possible the definition of realistic digital reconstructions directly starting from the experimental observation, allowing the definition of reverse engineering approaches (Rossi, 2025). This paper presents a wholly original theme regarding the identification, classification and description of the impact imprints generated by stone-throwers (ballistae) found in large numbers on the northern section of ancient Pompeii city walls (Fig. 1). Precisely because they were covered by a blanket of lapilli in 79 A.D. during the Vesuvio's eruption and brought to light some 19 centuries later, those footprints and traces are unequivocal and certain evidence of the actual potential of Republican artillery. Photogrammetric restitutions of the ballistic footprints, like the ones shown in Fig. 2, allow for the derivation of inverse models to be included as the origin of the experimentation on simulation models.-Once the high-resolution digital model has been detected (Bertacchi, 2025), thus obtaining the negative virtual cast of the existing wall surface, it is possible to derive (assisted by automated programs) the ideal volumes of the detected holes. The positive casts are similar to the impacting objects. In this case, spheroidal limestone balls. Given the stony consistency of the grey tuff or Sarno limestone (Kastenmeier, et al., 2010), it is possible to quantify the work required to pulverize the matter of known density and volume. Considering the initial throwing speed to be zero, the residual kinetic energy can be assimilated to the calculated work (Russo et al., 2025). The mechanical characterization will allow to ascertain the effects and therefore to trace the causes that, validated by the reverse engineering processes, will allow to certify the reconstructions of stone throwers. The objective in fact insists on the possibility of measuring and calibrating the modular components of the ante-Christ ballistae on the data collected along the northern stretch of the city walls, following the procedure indicated by Vitruvius (Book X of De Architettura) drawing on Greek texts (Rossi, 2024).This paper shows the first analysis of the characterization of wall, the modelling material response based on the literature, the simulation models for the case of the ballista, with mesh convergence, the estimation of impact velocity based on reported indentation depth and cavity profile, to perform calculation for drag using energy balance equation, estimate initial velocity and projectile angle. Object of experiment is a portion of the Northern part of the city walls of the ancient city of Pompei made of grey Nocera tuff, the ballistic spheres made of basalt, held in the antiquarium of the archaeological area.

Figure 1. Northern Section of Pompei's city Wall where the craters were found.

Figure 2. Examples of the craters found in the Northern Section of Pompei's City Walls.

2. 3D Survey

The walls and the cavities have been survey through photogrammetry using different cameras and lenses (Fig.3). For the entire structure, a full frame Canon 5D Mark III has been used coupled with a 20 mm lens, while for the cavities, a Canon 60D with a 60 mm macro lens and a Canon R6 mark II coupled with a 24 mm lens have been used. ISO and aperture have been set up accordingly considering the weather, conditions: when cloudy, ISO were set up on 800 and aperture to 5.6, during sunny days, ISO parameter was set up between 250 and 400 and aperture to 8 or superior. The choice of the different cameras was required by the dimensions and the positions of the different cavities: the macro lens was used for both spherical and quadrangular imprints, in a position close to operator, to acquire all their small details while the 24 mm for the ones in a higher position.
The entirety of the structure was also survey with a Leica ScanStation terrestrial laser scanner to scale and complete the photogrammetric survey. A total of 45 scan stations on a topographic reference network have been done to survey the 300 metres area between Vesuvio and Ercolano Gates. After the standard processing required to register the point clouds in a single local Cartesian coordinate system (using Leica Geosystems Cyclone software), the general models were referenced to the outer corner of Porta Vesuvio (origin point). In Figure 3 a complete map of the location of the ballistic marks un the wall adjoining the Vesuvio gate is shown.

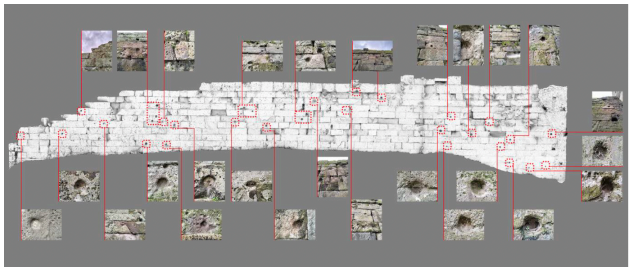

Figure 3. Location and photographs of the ballistic marks on the wall adjacent to the Vesuvio Gate.

Agisoft Metashape was used for the creation of the meshes that were then simplified with automatic retopology using Instant Meshes software. This passage was necessary to obtain a lighter and smoother model of each cavity that was then imported in Rhino to extrapolate profiles and create a NURBS model exported as volume, ready for FEA. The high-resolution mesh served as the basis for extracting significant geometric information from the cavities. The mesh was subjected to a light defeaturing and smart smoothing process, reducing noise and irregularities, and improving the uniformity of polygon faces, while preserving morphologically relevant features.
In addition, a more informative method was adopted to recreate the geometry based on dimensional observations and existing references. Using CAD tools, a series of 2D sketches were drawn on several planes (lines, n-sided polygons, etc.), utilising basic functions such as trimming, extending, or mirroring. These sketches were then used to create solid shapes through lofting, extrusion, or revolution operations of closed profiles, producing simplified yet plausible representations of the projectile. In Fig. 4 it is shown the process to reconstruct a stone projectile.

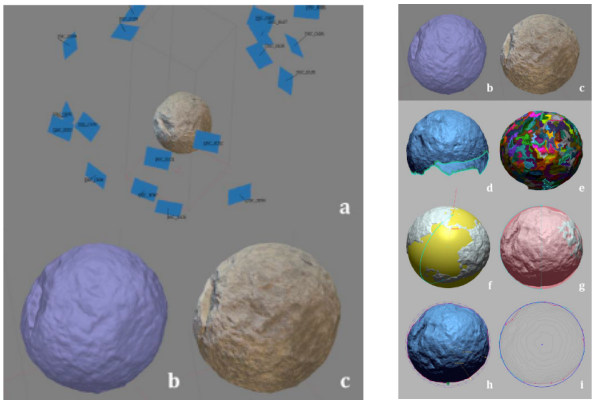

Figure 4. 3D model of a stone ball: (a) photogrammetric reconstruction, (b-c) polygonal mesh w/o and with texture, (d) edge trimming, (e) regionalization, (f) automatic primitive extraction, (g) radius of inscribed/circumscribed sphere, (h) best fitting circles from the 3D sections (Bertacchi, 2025).

3. Materials and Methods

This study aims to utilize Finite Element (FE) simulations to analyse ballistic impacts on the fortifications of Pompeii. By modelling the effects of Roman artillery, the research seeks to shed light on siege warfare dynamics, the structural resilience of ancient defences, and the effectiveness of Roman military technology. The findings will help clarify the relationship between limited material measurements, the characterization of Pompeii’s wall materials, and their overall response to ballistic impacts. Ultimately, the goal is to integrate historical analysis with modern computational tools to deepen our knowledge and understanding of these historical events. Initially, the relevant mechanical properties of Grey Tuff are compiled, and any missing parameters necessary for finite element modelling of impacts are calculated. Following this, the details of the developed model are described, including the geometries of the projectiles and wall sections, impact velocities, boundary conditions, and the material models used. Key parameters, including dimensions and material properties, are derived from a representative crater within the wall that was previously analysed and measured. The model is then used to simulate a systematically designed set of scenarios, examining how variations in impact angle affect the shape and size of the resulting indentation. These findings aim to enhance our understanding of Roman artillery, with particular emphasis on the performance of ballistae.

3.1 Material Characterization

The mechanical properties of Welded Grey Campania Tuff—such as elastic modulus and unconfined compressive strength (UCS)—have been extensively studied. UCS values range from 1.07 MPa to 11.68 MPa, with an average of 5.23 MPa (Piovesan, et al., 2019). Samples from the Campi Flegrei caldera showed UCS values of 10.59 MPa (dry) and 9.94 MPa (wet) (Manfredi et al., 2004). Another study reported a compressive stress of 4.47 MPa, which decreased to approximately 2.6 MPa at higher temperatures. The tangent modulus (Et), up to 50% of failure stress, is 2747 MPa, while the average (Em) and secant (Es) Young's moduli are 3495 MPa and 2790 MPa, respectively. Bending tests revealed UTS/UCS and E/UCS ratios of 0.286 and 561.9, respectively, indicating the material's flexural performance (Manfredi et al., 2004). Studies on Pompeii's water towers reported a density of 16 kN/m³ and a Young's modulus ranging from 800 MPa to 1800 MPa for Nocera Tuff (Lorenzoni et al., 2017). Additionally, research on the effects of pyroclastic flows on city walls identified a tuff wall density of 24 kN/m³ (Ruggeri et al., 2020). The static Young's modulus of Grey Tuff is approximately 1.5 GPa with a Poisson's ratio of 0.25, while dynamic properties suggest a Young's modulus around 2.5 GPa and a Poisson's ratio of 0.20 (Heap et al., (2014). Simulation studies have incorporated experimental fracture energy and axial stress data to better predict Grey Tuff's behaviour under various loads, enhancing model accuracy (Salvalaggio et al., 2017).
Numerical models calibrated for tensile and compressive stresses have been adjusted to reflect masonry's nonlinear behaviour, often using concrete properties for biaxial stress conditions (Nastri et al., 2023). The mechanical parameters of Grey Nocera Tuff, derived from existing literature and employed in the numerical simulations of the wall, are summarized in Table 1.

Parameter	Value	
UCS	4.47	MPa
E_{cm}	3495	MPa
E_{c1}	2511.7	MPa
α_α	E_{cm}/E_{c1}	-
α_d	0.4	-
E_s	2790	MPa
UTS/UCS	0.286	-
α_t	0.312·UTS	MPa

Table 1. Material parameters used for modelling Grey Nocera Tuff.

3.2 Material modelling

In the investigation of tuff masonry, especially within Italy's Campania region, the Finite Element Method (FEM) has demonstrated itself as an essential technique for simulating and examining mechanical performance. This method entails developing comprehensive models that integrate the material characteristics of tuff, including its compressive and tensile strengths, elastic modulus, and Poisson's ratio (Nastri et al., 2023). The modelling of tuff behaviour relies on the equations provided by (Nastri et al., 2023). When modelling tuff under compression, the following equations are employed:

Linear Elastic Region:

$$\sigma_c = E_{cm} \cdot \varepsilon \text{ for } \sigma_c \leq 50\% \, of \, UCS \quad (1)$$

Inelastic Region:

$$\sigma_c = UCS[\alpha_\alpha x + (3 - 2\alpha_\alpha)x^2 + (\alpha_\alpha - 2)x^3] \; for \; x \leq 1 \quad (2)$$

$$\sigma_c = UCS \cdot \frac{x}{\alpha_d \cdot (x-1)^2 + x} for \; x > 1 \quad (3)$$

where

$$x = \frac{\varepsilon}{\varepsilon_{c1}}; \alpha_\alpha = \frac{E_{cm}}{E_{c1}}; 0.4 \leq \alpha_d \leq 4; x_{max} = 10$$

For modelling tuff behaviour in tension, the equations used are as follows:

Linear elastic Region

$$\sigma_t = E_{cm} \cdot \varepsilon \text{ for } \sigma_t \leq UTS \quad (4)$$

Inelastic Region

$$\sigma_t = UTS \cdot \frac{x}{\alpha_t \cdot (x-1)^{1.7} + x} \quad (5)$$

for

$$x = \frac{\varepsilon}{\varepsilon_{c1}}; x_{max} = 5$$

The Concrete Damaged Plasticity (CDP) model is particularly effective for simulating the failure processes in masonry structures. The model accounts for two primary failure mechanisms: tensile cracking and compressive crushing. The evolution of material damage is governed by plastic deformation parameters, which are calibrated based on experimental data (Nastri et al., 2023)In the absence of specific experimental data, the input parameters for the biaxial failure surface in the CDP model are adopted from existing literature on concrete modelling. These five parameters—dilatation angle (Ψ), eccentricity (ε), the ratio σ_{b0}/σ_{c0}, K, and viscosity (μ)—are summarized in Table 2.

Ψ	ε	K	σ_{b0}/σ_{c0}	μ
20	0.1	0.5	1.16	0

Table 2. Plastic flow and yield function parameters

Furthermore, the progression of damage impacting inelastic, plastic, and crack strains is described by the equations below, with traction and compression damage values obtained from the selected stress–strain relationships. The material model also incorporates weight factors wt=0 and wc=1 to represent the degree of stiffness recovery during tension–compression and compression–tension transitions. These parameters play a crucial role in governing the unloading and reloading responses of the material under complex loading scenarios. For simulating damage behaviour during compression (Equations (6)–(8)) and tension (Equations (9)–(11)), the following equations are applied:

$$d_c = 1 - \frac{\sigma_i}{\sigma_{cu}}, \quad (6)$$

$$\varepsilon_c^{in} = \varepsilon_c - \varepsilon_c^{el}, \text{ where } \varepsilon_c^{el} = \frac{\sigma_c}{E_Y}; \quad (7)$$

$$\varepsilon_c^{pl} = \varepsilon_c^{in} - \frac{d_c}{(1-d_c)} \frac{\sigma_c}{E_Y}, \quad (8)$$

$$d_t = 1 - \frac{\sigma_i}{\sigma_{tu}}, \quad (9)$$

$$\varepsilon_t^{cr} = \varepsilon_t - \varepsilon_t^{el}, \text{ where } \varepsilon_t^{el} = \frac{\sigma_t}{E_Y}; \quad (10)$$

$$\varepsilon_t^{pl} = \varepsilon_t^{cr} - \frac{d_t}{(1-d_t)} \frac{\sigma_t}{E_Y}, \quad (11)$$

The flexibility of the CDP (Concrete Damage Plasticity) model allows it to accurately capture the nonlinear behaviour of masonry under both compression and tension, as shown in Figures 3a and 3b, respectively. When analysing wall panels, the CDP model is particularly effective at managing crack

development by linking the progression of failure to the extent of damage within the material. Nastri et al. have used and validated this approach by comparing it with experimental results, confirming its reliability in predicting the behaviour of tuff masonry structures (Nastri et al., 2023). The methodology used in this study is adapted from the work of (Nastri et al., 2023). Implementing this model requires defining the material behaviour separately under compression and tension. A maximum value of xmax = 10 is selected to represent complete material degradation. The parameters Ecm and Ec1 describe the material's response up to its ultimate compressive strength, including an initial linear elastic phase for stresses up to 0.5 UCS and a nonlinear stress–strain relationship approaching UCS. Additionally, the secant modulus ES is used to approximate the elastic response up to the material’s yield point. Fig. 5 illustrates the graphical representation of the constitutive equations for the materials modelled.

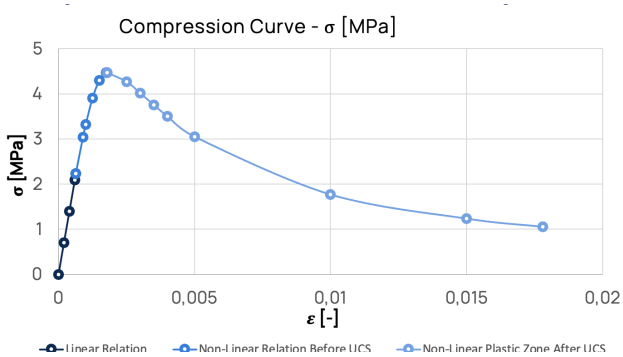

(a)

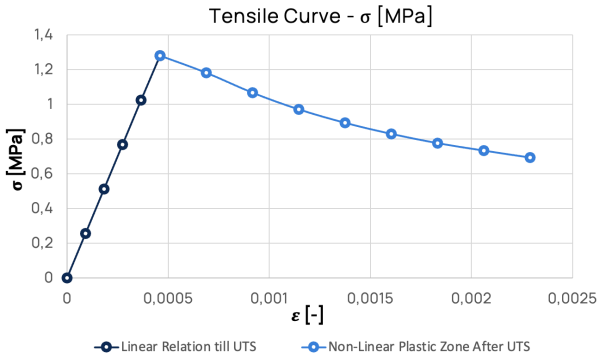

(b)

Figure 5. Stress vs. strain curve modelled using different parameters: (a) compression behaviour and (b) tensile behaviour.

For tensile stresses, a maximum value of x_{max} = 5 was used to accurately represent the brittle failure behaviour of tuff under tensile loading conditions. In this case, only linear elastic behaviour is considered up to the ultimate tensile strength (UTS), after which the material quickly fractures. Explicit methods are commonly favored for dynamic analyses or when simulating nonlinear material behavior, as they allow efficient handling of large-scale models while maintaining relatively short computation times. In this study, the explicit approach is appropriate due to the high-velocity ballistic impact involved in the simulation. The remaining general material properties of the tuff are listed in Table 3.

Parameter	Value	
Density	2297	kg/m^3
UCS	4.47	MPa
E_s	2.79	GPa
Poisson’s ratio	0.2	-

Table 3. Key parameters of tuff for the numerical simulation.

The projectile was modelled as a spherical basalt object exhibiting purely elastic behaviour. Due to basalt’s higher density, strength, and durability, it is more resistant to impact than the softer, more porous tuff, resulting in minimal deformation (Yan et al., 2012). Consequently, in this study, damage to the basalt projectile was neglected, and it was treated as a purely elastic material with the general properties listed in Table 4. The interaction between different bodies was defined considering a coefficient of friction equal to 0.4 for tangential interactions.

Parameter	Value	
Density	2520	kg/m^3
UCS	60	MPa
E_s	60	GPa
Poisson’s ratio	0.29	-

Table 4. Key parameters of Basalt projectile for the numerical simulation.

4. Numerical analysis

The simulation process was divided into two stages based on the dimensionality of the model. Mesh convergence and velocity–penetration depth analyses were conducted using a 2D axisymmetric model, which enabled faster simulations while preserving geometric accuracy for direct impacts. For simulations involving angular impacts, a full 3D model was employed to capture the crater asymmetric shape in the impact response at oblique angles and to precisely determine the width and depth of the resulting craters. The models were developed using Abaqus FEM software (Manual Abaqus, 2020) to simulate the impact of a basalt projectile on a tuff wall. The 3D model features a fully spherical projectile with a diameter of 140 mm, and a rectangular parallelepiped with dimensions of 3D (length) × 2D (width) × 1.5D (height), where D is the projectile’s diameter. The projectile size was chosen based on measurements from a crater observed in one of the studied wall sections, with measurement results shown in Figure 6a–b.

a

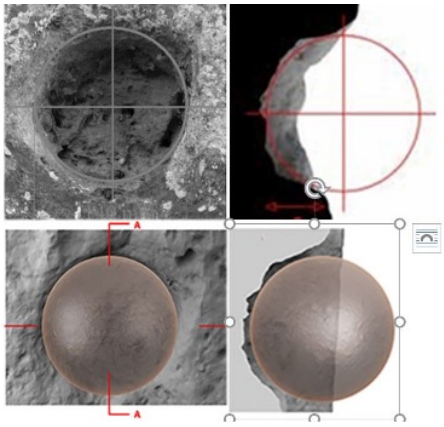

b

Figure 6. Spheroidal impact cavity (caused by stone balls): (a) Theoretical sphere. (b): above, the radius impact measured in 2002; below, renderings of the high-resolution digital models acquired in (Rossi, 2025).

The overall geometry of the model is illustrated in Figure 7.

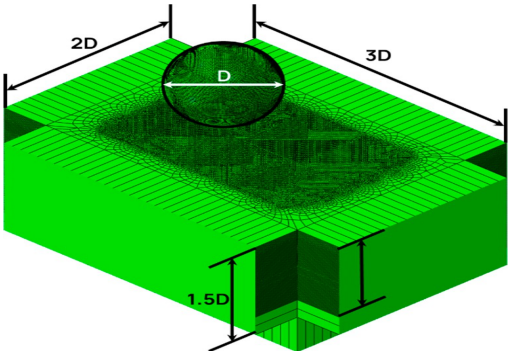

Figure 7. Finite Element model (Thakkar et al., 2025)..

The projectile and wall block were meshed using three-dimensional, eight-node brick elements with reduced integration and hourglass control (C3D8R). To represent an effectively distant boundary, a layer of infinite elements (CIN3D8R) was applied around all sides of the wall block. These elements serve as “quiet” boundaries in dynamic analyses (Ruggieri et al., 2020), helping to prevent stress wave reflections from the model’s edges and reducing size effects, thereby better representing the large dimensions of the actual wall. The developed model is then used for following analyses:

- A series of analyses with gradually decreasing element sizes were performed to evaluate mesh convergence, taking the projectile diameter (D) as the reference dimension. The mesh size was defined using a dividing factor, with D/100 identified as the optimal value for achieving convergence in damage energy. Although finer meshes provide greater stress accuracy, a mesh size of D/100 was deemed sufficient for accurately estimating penetration depth.
- Using the selected optimal mesh size, the model was employed to simulate a range of impact scenarios with velocities of 100 m/s, 80 m/s, 60 m/s, 40 m/s, 25 m/s, and 20 m/s. Among these, an impact velocity of 25 m/s produced a predicted penetration depth of 121 mm, closely aligning with the reference depth of 120 mm. Consequently, this velocity was chosen for the subsequent analyses. A series of analyses were carried out with angle of incidence gradually decreasing from 90◦ to 60◦ in 10◦ steps.

5. Results

5.1 Mesh convergence analysis

To accurately capture the interaction between the projectile and the tuff wall, a mesh convergence study was conducted. The characteristic dimensions—diameter (D) for the ball—served as reference lengths for determining appropriate mesh sizes. For various mesh size factors, FS = 100, corresponding to an element size of D/100, was identified as the optimal resolution for the ball impact model. As the mesh was refined, the resulting crater cavity appeared smoother and more detailed, with fewer surface irregularities and reduced element-based roughness. This enhancement in crater geometry clarity is illustrated in Figure 8. Although further refinement improved stress field resolution, it also increased computational costs without significantly enhancing the accuracy of penetration depth measurements. Therefore, D/100 was chosen as a balanced element size that optimized both efficiency and result fidelity.

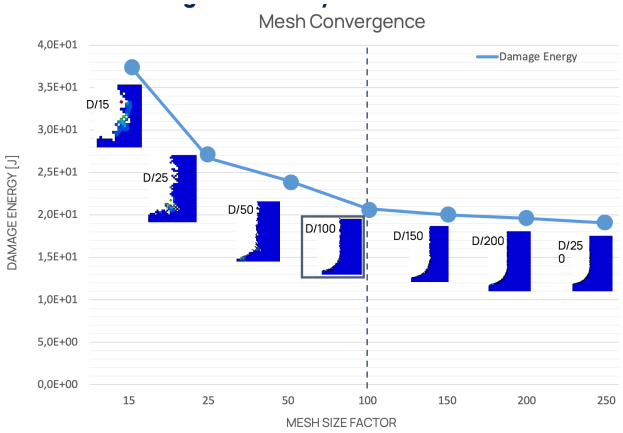

Figure 8. Mesh convergence analysis (Thakkar et al., 2025)..

5.2 Velocity range

To better understand the relationship between impact velocity and the resulting penetration depth, a series of detailed simulations were conducted. The primary goal was to identify the impact velocity at which the simulation outcomes align with archaeological observations of crater depths. Specifically, archaeological data indicate that the craters produced by the ball impacts are approximately 120 mm deep. By comparing these reference values with the results from our simulations, we aimed to determine the impact velocities that best replicate real-world damage patterns. For this purpose, a comprehensive set of simulations was performed focusing on the interaction between the ball and the tuff material. These simulations covered a broad range of impact velocities, from 20 meters per second (m/s) up to 100 m/s, to capture the full spectrum of possible impact scenarios. The crater depths resulting from each velocity were carefully recorded and are presented in Figure 9. The data clearly show that as impact velocity increases, the resulting crater depth also increases, but not in a linear fashion. Instead, the relationship appears to require progressively larger increases in impact velocity to produce proportional increases in crater depth. This suggests that the system's response becomes more sensitive at higher velocities. Among all the velocities tested, an impact velocity of approximately 25 m/s produced a crater depth that most closely matched the archaeological reference value of 120 mm. This finding is significant because it helps validate the simulation model and provides insight into the likely impact conditions that created the observed archaeological features. Overall, these simulations contribute valuable information for interpreting impact events and understanding the dynamics involved in crater formation on ancient structures or artifacts.

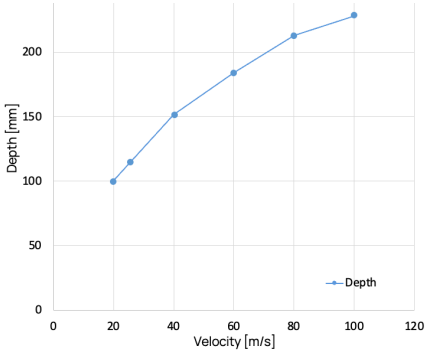

Figure 9. Trend of the penetration depth with respect of the impact velocity.

5.3 Angle of impact

A 3D simulation model was developed to analyse how Grey Tuff responds to impacts at various angles, using calibrated velocity of 25 m/s. Impact angles from 60° to 90° were considered, with 90° representing a normal hit. Dimple dimensions were assessed by measuring the displacement of the projectile’s centre of mass in both perpendicular and lateral directions from the impact surface. Figure 10 displays the crater width and depth as functions of the impact angle, indicating that the material’s response is similar in both cases. The following observations and analyses can be made regarding the impact dynamics and resulting crater morphology:

- Firstly, it is evident that the crater’s width and depth are directly influenced by the velocity components of the impacting object. Specifically, the horizontal and vertical components of velocity play a crucial role in determining these dimensions. The combined effect of these components can be quantitatively described by calculating the resultant velocity, which is obtained by taking the square root of the sum of the squares of the individual velocity components—essentially, applying the Pythagorean theorem. This resultant velocity correlates strongly with the observed penetration depth in impacts that occur perpendicular to the surface, indicating a consistent relationship between impact angle, velocity distribution, and crater morphology.
- Furthermore, this relationship implies that the material being impacted responds in a relatively uniform manner regardless of whether the impact occurs at an oblique or perpendicular angle. In other words, the material’s reaction—its resistance to penetration and its deformation characteristics—appears to be isotropic or directionally independent within the context of these impact scenarios. This uniform response suggests that factors such as material composition, density, and structural integrity dominate over directional effects when it comes to energy absorption and crater formation during impacts from different angles. Overall, understanding this relationship enhances our ability to predict crater dimensions based on impact velocities and angles, which is valuable for fields ranging from planetary geology to aerospace engineering.

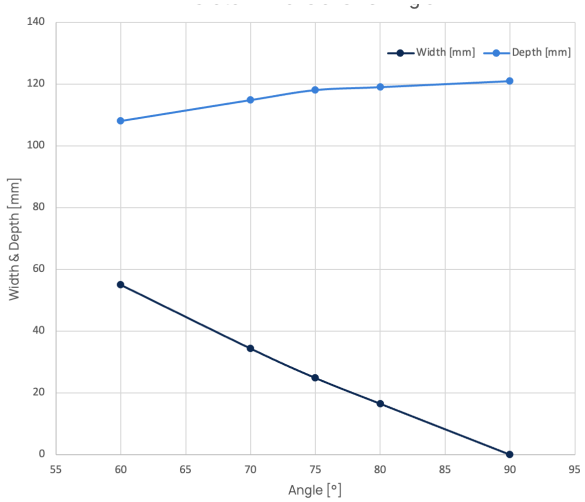

Figure 10. Dimple dimensions vs. the angle of impact.

In Figure 11 the craters that result with the different angles of impact are shown.

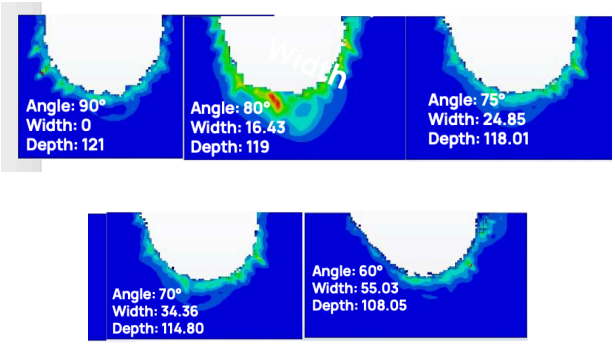

Figure 11. Crater's aspect with different angles of impact (width and depth in mm) (Thakkar et al., 2025)..

5.4 Discussion

By integrating experimental results, computational modelling, and simulation data, this methodology successfully characterized the impact resistance and failure mechanisms of Grey Campania Tuff under ballistic conditions.

5.4.1 Analysis of Impact Angles: Further insights were gained by examining how impact angles influence crater dimensions, specifically depth and width. The simulation results demonstrated a consistent relationship between the impact velocity components—namely, the normal (perpendicular) and tangential (parallel) parts—and the resulting crater features. By decomposing the impact velocity into these components, we observed that the combined magnitude, calculated as the square root of the sum of their squares, reliably correlated with the penetration depth observed in perpendicular impacts. This finding supports the idea that Grey Campania Tuff responds uniformly to impacts from different directions, with the overall impact energy being a key factor in determining crater size.

5.4.3 Material Behaviour Simulation: A crucial aspect of our modelling approach was accurately capturing the complex, nonlinear behaviour of Grey Campania Tuff under both compression and tension. The numerical methods employed proved effective in representing these behaviours, providing reliable parameters for further analysis. The simulation incorporated advanced constitutive models that account for the material’s response to stress, including damage accumulation and plastic deformation. This detailed material modelling ensures that the results are not only realistic but also useful for interpreting impact phenomena in archaeological contexts. Overall, these combined efforts—ranging from impact velocity assessment to impact angle analysis and material behaviour modelling—offer a comprehensive understanding of how Grey Campania Tuff responds to impacts. This knowledge is invaluable for reconstructing ancient impact events and understanding the formation of archaeological features such as craters and impact marks.

6. Conclusions

- To ensure the accuracy and reliability of these findings, we first conducted a comprehensive mesh convergence study. This analysis demonstrated that using a mesh size of D/100 for the projectile allowed us to produce smooth, realistic crater formations without imposing excessive computational demands. The relationship between impact velocity and penetration depth exhibited a nonlinear, nearly parabolic trend for both projectile types. For instance, a ball impacting at 25 m/s produced a penetration depth

of about 121 mm, closely matching the archaeological reference value of 120 mm observed in the field.These reference point served as critical benchmarks for subsequent simulations involving various impact angles, enabling us to develop a more comprehensive understanding of impact dynamics. Further analyses of oblique impacts revealed interesting patterns. As the impact angle decreased—that is, impacts became more oblique—the crater width tended to increase, while the penetration depth decreased proportionally. Interestingly, the overall displacement of the wall material remained nearly constant across different angles when considering the ball projectile, suggesting a uniform energy dissipation regardless of impact orientation. The arrow, with its pyramidal shape, exhibited slightly more variation in total displacement. This is likely due to its geometry, which influences how the volume of material engages during oblique impacts, affecting energy transfer and damage distribution. Additionally, 3D simulations of the ball projectile showed slightly reduced penetration depths compared to the simpler 2D axisymmetric models. This difference is probably due to lateral confinement effects and stress redistribution phenomena that are inherently captured in full 3D models but are absent in 2D approximations. These findings highlight the importance of three-dimensional modelling for more accurately capturing the complex behaviour of impacts. Overall, this research has led to the development of a robust and versatile 3D finite element (FE) model that accurately incorporates the material properties of Pompeii’s walls and simulates their response to various siege engine projectiles. The model was validated against documented experimental data and archaeological observations, ensuring its reliability. Such an FE framework can be employed to analyse wall reactions to impacts from different projectile shapes and materials, providing deeper insights into the design, effectiveness, and limitations of ancient Roman war machines. Ultimately, this work contributes to a more nuanced understanding of siege warfare tactics and the engineering resilience of ancient defensive structures.

Acknowledgments

This research was funded by the European Union—NextGenerationEU, M4C2 I1.1, Progetto PRIN 2022 “SCORPiò-NIDI”, Prot. 20222RJE32, CUP B53D23022100006 (DD n. 1012/2023), funded by the Ministry of Research under the PRIN call (DD call n. 104/2022). The authors wish to renew their gratitude to the management and officials in charge of the offices of the Archaeological Park of Pompeii for having issued the authorizations for access and investigation operations

7. References

Rossi, A. (Ed.), 2025: Discovering Pompeii: From Effects to Causes—From Surveying to the Reconstructions of Ballistae and Scorpiones” *Engineering Proceedings*, 96, https://www.mdpi.com/2673-4591/96/1.

Bertacchi, S., 2025: Primitive Shape Fitting of Stone Projectiles inSiegeWeapons: Geometric Analysis of Roman Artillery Ammunition. *Eng. Proc*., 96, 3. https://doi.org/10.3390/engproc2025096003

Kastenmeier P., Di Maio G., Balassone G., Boni M., Joachimski M., Mondillo N., 2010: The source of stone building materials from the Pompeii archaeological area and its surroundings. *Period. Mineral, Special Issue*, 39-58

Russo, F., Rossi, A., 2025: Ancient Science: From Effects to Ballistics Parameters. *Eng. Proc.,* 96, 2. https://doi.org/10.3390/engproc2025096002

Rossi, A. The Survey of the Ballistic Imprints for a Renewed Image of Unearthed Pompeii. Nexus Netw. J. 2024, 26, 307–324

Piovesan, R., Maritan, L., Meneghin, G., Previato, C., Baklouti, S., Sassi, R., Mazzoli, C., 2029: Stones of the façade of the Sarno Baths, Pompeii: A mindful construction choice. *J. Cult. Herit*, 40, 255–264.

Manfredi, G., Marcari, G., Voto, S., 2004: Analisi e caratterizzazione meccanica di murature di tufo. In Proceedings of the 15th CTE Congress, Bari, Italy, 4–6 November 2004; pp. 4–6.

Lorenzoni, F., Valluzzi, M.R., Salvalaggio, M., Minello, A., Modena, C., 2017: Operational modal analysis for the characterization of ancient water towers in Pompeii. *Procedia Eng*., 199, 3374–3379.

Ruggieri, N., Galassi, S., Tempesta, G., 2020: The effect of pyroclastic flows of the 79 AD eruption of Mount Vesuvius on the Pompeii’s city walls. The case study of the sector near the Tower XI. *J. Cult. Herit., 43, 235–241.*

Heap, M.J., Baud, P., Meredith, P.G., Vinciguerra, S., Reuschlé, T., 2014: The permeability and elastic moduli of tuff from Campi Flegrei, Italy: Implications for ground deformation modelling. *Solid Earth*, 5, 25–44.

Salvalaggio, M., Roca Fabregat, P., Valluzzi, M.R., Lorenzoni, F., 2017. Finite element micro-modelling for the characterization of inclined head joints archaeological masonry: The case of Villa Diomede in Pompeii. In Proceedings of the COMPDYN 2017—6th International Conference on Computational Methods in Structural Dynamics and Earthquake Engineering, Rhodes Island, Greece, 15–17 June 2017; National Technical University of Athens: Rhodes Island, Greece; pp. 2460–2469.

Nastri, E., Tenore, M., Todisco, P., 2023: Calibration of concrete damaged plasticity materials parameters for tuff masonry types of the Campania area. *Eng. Struct.*, 283, 115927.

Yan, F., Feng, X.T., Chen, R., Xia, K., Jin, C., 2012: Dynamic Tensile Failure of the Rock Interface Between Tuff and Basalt. Rock Mech. *Rock Eng.*, 45, 341–348.

A.U. Manual. Abaqus User Manual; Abaqus: New York, NY, USA, 2020.

Thakkar, M.M, Ardeshiri Lordejani, A., Guagliano, M., 2025: Structural Integrity Assessment of Pompeii’s City Wall Under Roman Artillery Fire: A Finite Element Approach. *Eng. Proc. 2025, 96, 7.*

Bertacchi, S., 2025: Primitive Shape Fitting of Stone Projectiles in Siege Weapons: Geometric Analysis of Roman Artillery Ammunition. *Eng. Proc. 2025, 96, 3.*